Electron-impact ionization of helium for equal-energy-sharing kinematics

A. T. Stelbovics, I. Bray, D. V. Fursa, and K. Bartschat*
Centre for Atomic, Molecular, and Surface Physics, Murdoch University, Perth 6150, Australia
(Received 12 January 2005; published 31 May 2005)

The close-coupling approach to electron-helium single ionization is analyzed and several ways of defining the scattering amplitudes are determined, for both equal- and unequal-energy outgoing electrons. Nevertheless, the various definitions all lead to the same cross section. The convergent close-coupling (CCC) method with Laguerre (CCC-L) and box-based (CCC-B) target functions is applied to calculate electron-impact ionization of helium for the cases where the two outgoing electrons have equal energy. Excellent absolute agreement with experiment is obtained for all available cases of comparison.

DOI: 10.1103/PhysRevA.71.052716 PACS number(s): 34.80.Dp

I. INTRODUCTION

The study of fully differential electron-impact single ionization of atoms at low to intermediate energies has spanned several decades. The key interest is in the behavior of three charged particles, two electrons and the residual ion, in the final state. In order to facilitate meaningful comparison between theory and experiment, the choice of the atomic target is very important. From the theoretical perspective, atomic hydrogen is ideal due to its analytically known wave functions. Though this is a particularly difficult target for the experimentalists, considerable effort has been expended in providing some absolute data for the *e*-H system [1–3], though much of the data are still available only on a relative scale [2]. The difficulty of putting the data on the absolute scale leads to large error bars, and some uncertainty in the near-threshold region remains [4–6]. Much qualitative understanding of the ionization process has been gained in comparison with theories that rely upon the asymptotic forms of the total wave function [7–11] and those based on the distorted-wave approach [2,12–16]. More recently, the emphasis has been on computationally intensive approaches that are capable of yielding complete absolute agreement with experiment. These concentrate on evaluating the final total wave function *ab initio*, such as the exterior complex scaling (ECS) approach [6,17,18], the time-dependent close-coupling method [19,20], and the convergent close-coupling (CCC) method [21–23]. Following the success of the numerical approaches, particularly the ECS method, the underlying formal theory of ionization has been reanalyzed leading to resolution of problems associated with divergence and ambiguity of the ionization amplitudes [24,25]. These ideas are not as readily applied to the CCC method, whose boundary conditions assume that only one electron is permitted to escape to infinity. This results in difficulties specific to the CCC method and we shall discuss them here in the context of *e*-He ionization.

Unlike atomic hydrogen, helium is a much more convenient target for the experimentalists. Consequently, there are a great deal more data available for the *e*-He single ionization system. These data generally have much smaller statistical error bars and have been mostly put on an absolute scale with considerably less uncertainty than in the case of the atomic hydrogen target [26–33]. For theorists, on the other hand, helium presents extra difficulties over atomic hydrogen in the treatment of the initial state and spin-coupling in the final state. Consequently, there have been fewer calculations published for this four-body system.

In recent times, only the CCC method has been extensively applied to the *e*-He fully differential single ionization problem. Following the successful implementation of the *e*-He CCC method [34] to *e*-He excitation processes [35], the method was extended to ionization with little extra effort required [21]. The four-body problem was reduced to an effective three-body one by ensuring that one of the helium electrons remained fixed and described by the He^+ 1*s* orbital throughout the collision process. Ionization was treated in exactly the same way as excitation, except that it was associated with positive-energy pseudostates. Such an approach proved most promising [36], but some computational and formal difficulties were identified [37]. Specifically, for a given ionization process with outgoing electrons of energies $k_B^2/2 < k_A^2/2$, the CCC method yields two independent amplitudes $f(\boldsymbol{k}_A, \boldsymbol{k}_B)$ and $f(\boldsymbol{k}_B, \boldsymbol{k}_A)$ arising from excitation of open pseudostates with energy $\epsilon_{nl} = k_B^2/2$ and $\epsilon_{n'l} = k_A^2/2$, respectively. Yet the theory is unitary and yields excellent agreement with the measurements of the total ionization cross sections obtained by summing over the excitation cross sections for all positive-energy pseudostates [21,38]. In other words, there appears to be a double-counting problem within a unitary theory. Based upon computational studies, a resolution of this problem was suggested by claiming that, as the close-coupling expansion was taken to completeness, the $f(\boldsymbol{k}_B, \boldsymbol{k}_A)$ term would converge to zero [37]. Although this step-function hypothesis has yet to be proven directly, it is consistent with the numerical behavior of the CCC calculations. Furthermore, it was suggested that the CCC amplitudes behaved as a Fourier expansion of a step function with convergence at the equal-energy point to half the step height [39]. This led to the explanation as to why the cross-section prescription given by [21] yielded results for asymmetric energy sharing that oscillated slightly with increasing basis size *N*, and were too low by a factor of 2 at the equal-energy-sharing point [40,41]. In this work, we expand on the pre-

*Permanent address: Department of Physics and Astronomy, Drake University, Des Moines, IA 50311, USA.

liminary report [41] of electron-impact single ionization of helium in the equal-energy-sharing regime, and apply it extensively to the available experimental data.

II. COUPLED-CHANNEL EXPANSIONS

Electron-helium scattering can be accurately described within the nonrelativistic formulation adopted in this work. In nonrelativistic quantum mechanics, spin and space coordinates can be separated, and the total spin S of the electron-helium scattering system is a conserved quantum number. Denoting the three electrons in our collision system by "0," "1," and "2" for the projectile and the two target electrons, the general coupled-channel expansion over the discrete spectrum $\Phi_{s\mu\gamma}(1,2)$ and the continuum $\Phi^{(-)}_{s\mu\boldsymbol{q}}(1,2)$ target states for our case of interest is given by

$$\Psi^{(+)}_{SM_S}(0,1,2) = \frac{2}{\sqrt{3!}}(1 - P_{01} - P_{02}) \times \sum_{s\mu\mu_0}\left[\sum_{\gamma} \mathcal{G}^{(+)SM_S}_{s\mu\mu_0\gamma}(0)\Phi_{s\mu\gamma}(1,2) + \int dq^3 \mathcal{G}^{(+)SM_S}_{s\mu\mu_0\boldsymbol{q}}(0)\Phi^{(-)}_{s\mu\boldsymbol{q}}(1,2)\right], \quad (1)$$

where the functions $\mathcal{G}^{(+)SM_S}_{s\mu\mu_0\gamma}$ include both space and spin coordinates and the permutation operator P_{ij} interchanges the electrons "i" and "j." The sum is over the target spin quantum numbers μ and s and the projectile magnetic spin quantum numbers μ_0.

In what follows, we are interested in the part of the close-coupling expansion (1) that corresponds to ionization, and hence we will drop the first term in Eq. (1) for brevity of notation. The helium continuum states in Eq. (1) are accurately described by the frozen-core model. In this model, one of the electrons in the helium atom is fixed in the He^+ $1s$ orbital, and the antisymmetric two-electron continuum wave function with energy e_{sq} is

$$\Phi^{(-)}_{s\mu\boldsymbol{q}}(1,2) = \frac{1}{\sqrt{2}}(1 - P_{12})\phi^{(-)}_{s\boldsymbol{q}}(\boldsymbol{r}_1)u(\boldsymbol{r}_2)\chi_{s\mu}(12), \quad (2)$$

where $\chi_{s\mu}(12)$ is the two-electron spin function with spin quantum numbers s and μ, $u(\boldsymbol{r})$ is the He^+ $1s$ orbital, and $\phi^{(-)}_{s\boldsymbol{q}}(\boldsymbol{r})$ is a continuum one-electron orbital with momentum $\boldsymbol{q}$. The spatial part of the helium wave function can be written as

$$\Phi^{(-)}_{s\boldsymbol{q}}(\boldsymbol{r}_1,\boldsymbol{r}_2) = \frac{1}{\sqrt{2}}[1 + (-1)^s P_{r_1r_2}]\phi^{(-)}_{s\boldsymbol{q}}(\boldsymbol{r}_1)u(\boldsymbol{r}_2), \quad (3)$$

where $P_{r_1r_2}$ is the space exchange operator.

By energy conservation, we have

$$k_i^2/2 + e_i = k^2/2 + q^2/2 - 2 = E - 2, \quad (4)$$

where $\boldsymbol{k}_i$ is the initial electron momentum, e_i is the energy of the initial He state, $\boldsymbol{k}$ is a final electron momentum, and the energy of the He^+ $1s$ orbital is -2 a.u. Often E is referred to as the excess energy.

Separating the spin and space coordinates, we can write the target-state expansion in Eq. (1) in the spin-coupled form,

$$\sum_{\mu_0\mu} \mathcal{G}^{(+)SM_S}_{s\mu_{12}\mu_0\boldsymbol{q}}(0)\Phi^{(-)}_{s\mu\boldsymbol{q}}(1,2) = \sum_{\mu_0\mu} \chi^{\frac{1}{2}\mu_0}(0)\chi_{s\mu}(12) \times \left(\frac{1}{2}s,\mu_0\mu|SM_S\right) G^{(+)S}_{s\boldsymbol{q}}(\boldsymbol{r}_0) \times \Phi^{(-)}_{s\boldsymbol{q}}(\boldsymbol{r}_1,\boldsymbol{r}_2), \quad (5)$$

where $G^{(+)S}_{s\boldsymbol{q}}(\boldsymbol{r}_0)\Phi^{(-)}_{s\boldsymbol{q}}(\boldsymbol{r}_1,\boldsymbol{r}_2)$ is only a function of the radial coordinates $\boldsymbol{r}_0$, $\boldsymbol{r}_1$, and $\boldsymbol{r}_2$. For brevity we introduce the spin-coupled functions

$$\chi_{sSM_S}(0,1,2) = \sum_{\mu_0\mu} \chi^{\frac{1}{2}\mu_0}(0)\chi_{s\mu}(12)\left(\frac{1}{2}s,\mu_0\mu|SM_S\right). \quad (6)$$

Hence, in the case of ionization,

$$\Psi^{(+)}_{SM_S}(0,1,2) = \sqrt{\frac{2}{3}}(1 - P_{01} - P_{02})\sum_s \int dq^3 \chi_{sSM_S}(0,1,2) \times G^{(+)S}_{s\boldsymbol{q}}(\boldsymbol{r}_0)\Phi^{(-)}_{s\boldsymbol{q}}(\boldsymbol{r}_1,\boldsymbol{r}_2). \quad (7)$$

The effect of the permutation operators P_{01} and P_{02} is evaluated by using the fact that the spin functions χ_{sSM_S} form a complete set. Hence

$$\chi_{sSM_S}(2,1,0) = \sum_{s'} \chi_{s'SM_S}(0,1,2) \times \langle \chi_{s'SM_S}(0,1,2)|\chi_{sSM_S}(2,1,0)\rangle = \sum_{s'} \alpha_{ss'S}\chi_{s'SM_S}(0,1,2), \quad (8)$$

$$\chi_{sSM_S}(1,0,2) = \sum_{s'} \alpha_{ss'S}(-1)^{s+s'}\chi_{s'SM_S}(0,1,2), \quad (9)$$

where the recoupling coefficients are given by the 6j symbol

$$\alpha_{ss'S} = -\hat{s}\hat{s}'\begin{Bmatrix} \frac{1}{2} & \frac{1}{2} & s \\ \frac{1}{2} & S & s' \end{Bmatrix}, \quad (10)$$

and $\hat{x} \equiv \sqrt{2x+1}$. The explicit values of interest here are

$$\alpha_{00\frac{1}{2}} = \frac{1}{2}, \quad \alpha_{11\frac{1}{2}} = -\frac{1}{2}, \quad \alpha_{11\frac{3}{2}} = 1,$$

$$\alpha_{01\frac{1}{2}} = \alpha_{10\frac{1}{2}} = -\frac{\sqrt{3}}{2}. \quad (11)$$

From the properties of the 6j symbols, we obtain the relation

$$\sum_s \alpha_{ss'S}\alpha_{ss''S} = \delta_{s's''}. \quad (12)$$

We now write the ionization part of the close-coupling expansion (1) using spin recoupling in the following form:

$$\Psi^{(+)}_{SM_S}(0,1,2) = \sqrt{\frac{2}{3}}\sum_{ss'}\int dq^3\{\delta_{ss'}G^{(+)S}_{s\boldsymbol{q}}(\boldsymbol{r}_0)\Phi^{(-)}_{s\boldsymbol{q}}(\boldsymbol{r}_1,\boldsymbol{r}_2) - \alpha_{ss'S}(-1)^{s+s'}G^{(+)S}_{s\boldsymbol{q}}(\boldsymbol{r}_1)\Phi^{(-)}_{s\boldsymbol{q}}(\boldsymbol{r}_0,\boldsymbol{r}_2) - \alpha_{ss'S}G^{(+)S}_{s\boldsymbol{q}}(\boldsymbol{r}_2)\Phi^{(-)}_{s\boldsymbol{q}}(\boldsymbol{r}_1,\boldsymbol{r}_0)\}\chi_{sSM_S}(0,1,2). \tag{13}$$

The proper scattering boundary conditions for the distorted waves $G^{(+)S}$ for elastic scattering and excitation of a helium bound state from an initial state "i" are

$$G^{(+)S}_{s\gamma_n}(\boldsymbol{r}) \underset{r\to\infty}{\to} \delta_{ss_i}\delta_{\gamma_n\gamma_i}e^{i\boldsymbol{k}_i\cdot\boldsymbol{r}} + f^S_{s\gamma_n s_i\gamma_i}(\boldsymbol{k}_i)\frac{e^{ik_n r}}{r}, \tag{14}$$

and in the case of excitation of a continuum state "q"

$$G^{(+)S}_{s\boldsymbol{q}}(\boldsymbol{r}) \underset{r\to\infty}{\sim} f^S_{ss_i\gamma_i}(\boldsymbol{k},\boldsymbol{q};\boldsymbol{k}_i)\frac{e^{ikr}}{r}. \tag{15}$$

The calculation of the amplitudes $f^S_{ss_i\gamma_i}(\boldsymbol{k},\boldsymbol{q};\boldsymbol{k}_i)$ has been detailed in Ref. [21]. Note that the step-function hypothesis [37] states that these should be nonzero only for $q \leqslant k$.

We consider the asymptotic form of $\Psi^{(+)}_{SM_S}(0,1,2)$ in the limit of $r_0, r_1 \to \infty$. The $\Phi^{(-)}_{s\boldsymbol{q}}(\boldsymbol{r}_1,\boldsymbol{r}_0)$ term vanishes from Eq. (13) because of our assumption that one of the electrons is in the He^+ ground state and hence is described by an exponentially decreasing wave function. In the remaining terms, we only get contributions from the target waves when neither electron 0 nor 1 is in the 1s orbital. Hence,

$$\Psi^{(+)}_{SM_S}(0,1,2) \underset{r_0,r_1\to\infty}{\sim} \sqrt{\frac{2}{3}}\sum_{ss'}\chi_{s'SM_S}(0,1,2)\int_0^{\sqrt{2E}} d^3q\left\{\delta_{ss'}f^S_{ss_i\gamma_i}(\boldsymbol{k},\boldsymbol{q};\boldsymbol{k}_i)\frac{e^{ikr_0}}{r_0} \times\frac{1}{\sqrt{2}}u(\boldsymbol{r}_2)\phi^{(-)}_{\boldsymbol{q}}(\boldsymbol{r}_1) + (-1)^{1+s+s'}\alpha_{ss'S}f^S_{ss_i\gamma_i}(\boldsymbol{k},\boldsymbol{q};\boldsymbol{k}_i)\frac{e^{ikr_1}}{r_1}\frac{1}{\sqrt{2}}u(\boldsymbol{r}_2)\phi^{(-)}_{\boldsymbol{q}}(\boldsymbol{r}_0)\right\}. \tag{16}$$

Now let us consider the above integrals further. The continuum waves in the first term are $e^{ikr_0}\phi^{(-)}_{\boldsymbol{q}}(\boldsymbol{r}_1)/r_0$ and similarly in the second term, except for $\boldsymbol{r}_0$ and $\boldsymbol{r}_1$ interchanged. We now use the outgoing spherical-wave component of $\phi^{(-)}_{\boldsymbol{q}}$ [see Eq. (52) in the Appendix] and evaluate the angular integrals in Eq. (16) to yield

$$\Psi^{(+)}_{SM_S}(0,1,2) \underset{r_0,r_1\to\infty}{\sim} \sqrt{\frac{1}{3}}u(\boldsymbol{r}_2)\frac{(2\pi)^{-1/2}}{i}\sum_{ss'}\chi_{s'SM_S}(0,1,2)\int_0^{\sqrt{2E}} dq\left\{\delta_{ss'}\frac{q}{r_0r_1}e^{i(kr_0+qr_1)}e^{i(1/q)\ln(2qr_1)}f^S_{ss_i\gamma_i}(k\hat{\boldsymbol{r}}_0,q\hat{\boldsymbol{r}}_1;\boldsymbol{k}_{s_i\gamma_i}) + \frac{q}{r_0r_1}e^{i(kr_1+qr_0)}e^{i(1/q)\ln(2qr_0)}(-1)^{1+s+s'}\alpha_{ss'S}f^S_{ss_i\gamma_i}(k\hat{\boldsymbol{r}}_1,q\hat{\boldsymbol{r}}_0;\boldsymbol{k}_{s_i\gamma_i})\right\}. \tag{17}$$

We evaluate the integrals by the stationary phase method as discussed in the Appendix. The stationary point for the first term will be at $q/k = r_1/r_0$. Note that q and k in Eq. (17) are related by energy conservation: $2E = q^2 + k^2$. We will denote the stationary point for q by k_b and the corresponding point for k by k_a. In the second term, the stationary point will be at $k/q = r_0/r_1$ and this stationary point for q corresponds to the value k_a in the first term. Hence, the contribution to the first amplitude is $f^S_{ss_i\gamma_i}(k_a\hat{\boldsymbol{r}}_0, k_b\hat{\boldsymbol{r}}_1;\boldsymbol{k}_i)$ while the amplitude in the second term will be $f^S_{ss_i\gamma_i}(k_b\hat{\boldsymbol{r}}_1, k_a\hat{\boldsymbol{r}}_0;\boldsymbol{k}_i)$. The result is

$$\Psi^{(+)}_{SM_S}(0,1,2) \underset{r_0,r_1\to\infty}{\sim} \sqrt{\frac{1}{3}}u(\boldsymbol{r}_2)\frac{K^{3/2}}{iR^{5/2}}e^{i(KR-\pi/4)}\sum_{ss'}\chi_{s'SM_S}(0,1,2) \times\{\delta_{ss'}e^{i(1/k_b)\ln(2k_br_1)}f^S_{ss_i\gamma_i}(k_a\hat{\boldsymbol{r}}_0,k_b\hat{\boldsymbol{r}}_1;\boldsymbol{k}_i) + e^{i(1/k_a)\ln(2k_ar_0)}(-1)^{1+s+s'}\alpha_{ss'S} \times f^S_{ss_i\gamma_i}(k_b\hat{\boldsymbol{r}}_1,k_a\hat{\boldsymbol{r}}_0;\boldsymbol{k}_i)\}, \tag{18}$$

where we have introduced the hyperspherical coordinates

$$R^2 = r_0^2 + r_1^2, \quad \tan\alpha = r_1/r_0, \tag{19}$$

$$r_0 = R\cos\alpha, \quad r_1 = R\sin\alpha, \tag{20}$$

$$K^2 = k_a^2 + k_b^2. \tag{21}$$

Note that the stationary point condition $k_b/k_a = r_1/r_0$ together with the above definitions leads to the relation $k_b/r_1 = k_a/r_0 = K/R$.

We can see from Eq. (18) that the logarithmic phase factors generally do not allow us to define an ionization amplitude, except for the case of equal energy sharing, $k_a = k_b = k$, where the asymptotic of the wave function takes the following form:

$$\Psi^{(+)}_{SM_S}(0,1,2) \underset{r_0,r_1\to\infty}{\sim} \sqrt{\frac{1}{3}}u(\boldsymbol{r}_2)\frac{K^{3/2}}{R^{5/2}}e^{i(KR-3\pi/4)}e^{i(1/k)\ln(KR)} \times \sum_{s'} \chi_{s'SM_S}(0,1,2)F^S_{s',s_i\gamma_i}(k\hat{\boldsymbol{r}}_0,k\hat{\boldsymbol{r}}_1;\boldsymbol{k}_i). \tag{22}$$

Here the amplitude is defined as

$$F^S_{s,s_i\gamma_i}(k\hat{\boldsymbol{r}}_0,k\hat{\boldsymbol{r}}_1;\boldsymbol{k}_i) = f^S_{ss_i\gamma_i}(k\hat{\boldsymbol{r}}_0,k\hat{\boldsymbol{r}}_1;\boldsymbol{k}_i) + \sum_{s'}(-1)^{1+s+s'} \times \alpha_{ss'S}f^S_{s's_i\gamma_i}(k\hat{\boldsymbol{r}}_1,k\hat{\boldsymbol{r}}_0;\boldsymbol{k}_i), \tag{23}$$

or, specifically for the case of interest, $S=1/2$, $s_i=0$, and the initial state γ_i, which we now drop from the notation

$$F_0(k\hat{\boldsymbol{r}}_0,k\hat{\boldsymbol{r}}_1;\boldsymbol{k}_i) = f_0(k\hat{\boldsymbol{r}}_0,k\hat{\boldsymbol{r}}_1;\boldsymbol{k}_i) - \frac{1}{2}f_0(k\hat{\boldsymbol{r}}_1,k\hat{\boldsymbol{r}}_0;\boldsymbol{k}_i) - \frac{\sqrt{3}}{2}f_1(k\hat{\boldsymbol{r}}_1,k\hat{\boldsymbol{r}}_0;\boldsymbol{k}_i) \tag{24}$$

and

$$F_1(k\hat{\boldsymbol{r}}_0,k\hat{\boldsymbol{r}}_1;\boldsymbol{k}_i) = f_1(k\hat{\boldsymbol{r}}_0,k\hat{\boldsymbol{r}}_1;\boldsymbol{k}_i) - \frac{\sqrt{3}}{2}f_0(k\hat{\boldsymbol{r}}_1,k\hat{\boldsymbol{r}}_0;\boldsymbol{k}_i) + \frac{1}{2}f_1(k\hat{\boldsymbol{r}}_1,k\hat{\boldsymbol{r}}_0;\boldsymbol{k}_i). \tag{25}$$

For the case of asymmetric energy sharing, the $f^S_{s's_i\gamma_i}(k_b\hat{\boldsymbol{r}}_1,k_a\hat{\boldsymbol{r}}_0;\boldsymbol{k}_i)$ tend to zero with increasing basis sizes for $k_b<k_a$. In this case, we can always define the amplitude from Eq. (18), and it is simply

$$F_s(k_a\hat{\boldsymbol{r}}_0,k_b\hat{\boldsymbol{r}}_1;\boldsymbol{k}_i) = f_s(k_a\hat{\boldsymbol{r}}_0,k_b\hat{\boldsymbol{r}}_1;\boldsymbol{k}_i), \quad k_b<k_a. \tag{26}$$

The amplitudes (23) satisfy a certain symmetry relation on interchange of $k\hat{\boldsymbol{r}}_1$ and $k\hat{\boldsymbol{r}}_0$. This relation, first given in Eq. (9) of [41], can be obtained by considering the antisymmetry property of the asymptotic wave function (23), $\Psi^{(+)}_{SM_S}(1,0,2)=-\Psi^{(+)}_{SM_S}(0,1,2)$, with the result

$$F_s(k\hat{\boldsymbol{r}}_0,k\hat{\boldsymbol{r}}_1;\boldsymbol{k}_i) = -\sum_{s'}(-1)^{s+s'}\alpha_{ss'S}F_{s'}(k\hat{\boldsymbol{r}}_1,k\hat{\boldsymbol{r}}_0;\boldsymbol{k}_i). \tag{27}$$

A similar procedure to the one outlined above for $r_0,r_2\to\infty$ yields

$$\Psi^{(+)}_{SM_S}(0,1,2) \underset{r_0,r_2\to\infty}{\sim} \sqrt{\frac{1}{3}}u(\boldsymbol{r}_1)\frac{K^{3/2}}{R^{5/2}}e^{i(KR-3\pi/4)}e^{i(1/k)\ln(KR)} \times \sum_{ss'}\{\delta_{ss'}(-1)^s f^S_{ss_i\gamma_i}(k\hat{\boldsymbol{r}}_0,k\hat{\boldsymbol{r}}_2;\boldsymbol{k}_i) - (-1)^s \times \alpha_{ss'S}f^S_{ss_i\gamma_i}(k\hat{\boldsymbol{r}}_2,k\hat{\boldsymbol{r}}_0;\boldsymbol{k}_i)\}\chi_{s'SM_S}(0,1,2). \tag{28}$$

Comparing this expression with Eq. (23) for $r_0,r_1\to\infty$, we observe that the amplitudes can be defined in a similar way with only a phase difference in the triplet amplitude (25). As we will see shortly, a calculation of cross sections involves only the absolute values of the singlet and triplet amplitudes, and hence this phase difference does not affect the cross-section results.

Finally, for $r_1,r_2\to\infty$ we find

$$\Psi^{(+)}_{SM_S}(0,1,2) \underset{r_1,r_2\to\infty}{\sim} -\sqrt{\frac{1}{3}}u(\boldsymbol{r}_0)\frac{K^{3/2}}{R^{5/2}}e^{i(KR-3\pi/4)} \times e^{i(1/k)\ln(KR)}\sum_{ss'}\{(-1)^{s'}f^S_{ss_i\gamma_i}(k\hat{\boldsymbol{r}}_1,k\hat{\boldsymbol{r}}_2;\boldsymbol{k}_i) + f^S_{ss_i\gamma_i}(k\hat{\boldsymbol{r}}_2,k\hat{\boldsymbol{r}}_1;\boldsymbol{k}_i)\}\alpha_{ss'S}\chi_{s'SM_S}(0,1,2), \tag{29}$$

and the amplitudes can be defined as

$$F'_s(k\hat{\boldsymbol{r}}_1,k\hat{\boldsymbol{r}}_2;\boldsymbol{k}_i) = \sum_{s'}\{(-1)^s f^S_{s's_i\gamma_i}(k\hat{\boldsymbol{r}}_1,k\hat{\boldsymbol{r}}_2;\boldsymbol{k}_i) + f^S_{s's_i\gamma_i}(k\hat{\boldsymbol{r}}_2,k\hat{\boldsymbol{r}}_1;\boldsymbol{k}_i)\}\alpha_{ss'S}. \tag{30}$$

It can be verified that these amplitudes satisfy the following symmetry relation under interchange of $k\hat{\boldsymbol{r}}_1$ and $k\hat{\boldsymbol{r}}_2$:

$$F'_s(k\hat{\boldsymbol{r}}_1,k\hat{\boldsymbol{r}}_2;\boldsymbol{k}_i) = (-1)^s F'_s(k\hat{\boldsymbol{r}}_2,k\hat{\boldsymbol{r}}_1;\boldsymbol{k}_i). \tag{31}$$

As before, for the case of interest, the amplitude (30) leads to

$$F'_0(k\hat{\boldsymbol{r}}_1,k\hat{\boldsymbol{r}}_2;\boldsymbol{k}_i) = \frac{1}{2}\{f_0(k\hat{\boldsymbol{r}}_1,k\hat{\boldsymbol{r}}_2;\boldsymbol{k}_i) + f_0(k\hat{\boldsymbol{r}}_2,k\hat{\boldsymbol{r}}_1;\boldsymbol{k}_i)\} - \frac{\sqrt{3}}{2}\{f_1(k\hat{\boldsymbol{r}}_1,k\hat{\boldsymbol{r}}_2;\boldsymbol{k}_i) + f_1(k\hat{\boldsymbol{r}}_2,k\hat{\boldsymbol{r}}_1;\boldsymbol{k}_i)\} \tag{32}$$

and

$$F'_1(k\hat{\boldsymbol{r}}_1,k\hat{\boldsymbol{r}}_2;\boldsymbol{k}_i) = \frac{\sqrt{3}}{2}\{f_0(k\hat{\boldsymbol{r}}_1,k\hat{\boldsymbol{r}}_2;\boldsymbol{k}_i) - f_0(k\hat{\boldsymbol{r}}_2,k\hat{\boldsymbol{r}}_1;\boldsymbol{k}_i)\} + \frac{1}{2}\{f_1(k\hat{\boldsymbol{r}}_1,k\hat{\boldsymbol{r}}_2;\boldsymbol{k}_i) - f_1(k\hat{\boldsymbol{r}}_2,k\hat{\boldsymbol{r}}_1;\boldsymbol{k}_i)\}, \tag{33}$$

We can see that the amplitudes defined in Eqs. (24) and (25) for $r_0,r_1\to\infty$ differ from the above amplitudes obtained for $r_1,r_2\to\infty$. However, after some algebra we find that $|F_0|^2+|F_1|^2=|F'_0|^2+|F'_1|^2$.

For asymmetric energy sharing with $k_b<k_a$, we again use the step-function hypothesis [37] and obtain from Eqs. (32) and (33)

$$F'_0(k_a\hat{\boldsymbol{r}}_1,k_b\hat{\boldsymbol{r}}_2;\boldsymbol{k}_i) = \frac{1}{2}f_0(k_a\hat{\boldsymbol{r}}_1,k_b\hat{\boldsymbol{r}}_2;\boldsymbol{k}_i) - \frac{\sqrt{3}}{2}f_1(k_a\hat{\boldsymbol{r}}_1,k_b\hat{\boldsymbol{r}}_2;\boldsymbol{k}_i) \tag{34}$$

and

$$F_1'(k_a\hat{\boldsymbol{r}}_1,k_b\hat{\boldsymbol{r}}_2;\boldsymbol{k}_i)=\frac{\sqrt{3}}{2}f_0(k_a\hat{\boldsymbol{r}}_1,k_b\hat{\boldsymbol{r}}_2;\boldsymbol{k}_i)+\frac{1}{2}f_1(k_a\hat{\boldsymbol{r}}_1,k_b\hat{\boldsymbol{r}}_2;\boldsymbol{k}_i). \tag{35}$$

This is different from that obtained previously [see the note following Eq. (25)], but once more $|F_0|^2+|F_1|^2=|F_0'|^2+|F_1'|^2$.

Let us now turn to the calculation of the cross section for ionization. We consider the $r_0,r_1\to\infty$ limit as both $r_0,r_2\to\infty$ and $r_1,r_2\to\infty$ asymptotic limits lead to the same cross-section result. Following [42], we consider the probability flux through a small section $dS=R^5d\Omega$ of a remote six-dimensional hypersphere,

$$dN=J_RdS=J_RR^5d\Omega, \tag{36}$$

where Ω denotes a direction in six-dimensional configuration space, and

$$d\Omega=d\Omega_0d\Omega_1\sin^2\alpha\cos^2\alpha d\alpha=d\Omega_0d\Omega_1\frac{k_ak_b}{K^4}de_b, \tag{37}$$

where $e_b=k_b^2/2$ is the continuum electron energy. The radial component of the six-dimensional flux density is defined as

$$J_R=\mathrm{Im}\left(\int d^3r_2\Psi_{SM_S}^{(+)*}\frac{\partial}{\partial R}\Psi_{SM_S}^{(+)}\right). \tag{38}$$

It can be evaluated using Eq. (23) for the asymptotic wave function, with the result

$$J_R=\frac{1}{3}\frac{K^4}{R^5}\sum_s|F_{s,s_i\gamma_i}^S|^2. \tag{39}$$

To calculate the cross section, this flux needs to be multiplied by 2 (the number of electrons in helium), and the cross-section, differential in angles and energy of the continuum electrons becomes

$$d\sigma=dN/J_0=\frac{k_ak_b}{k_i}\sum_s|F_{s,s_i\gamma_i}^S|^2d\Omega_0d\Omega_1de_b, \tag{40}$$

where $J_0=2k_i/3$ is the initial flux. Note that, unlike in Eq. (27) of Ref. [21], we have absorbed the factor of $(2\pi)^2$ in the amplitudes.

To finish this section, we recall the result Eq. (12) of the earlier work [41], that at equal energy-sharing, with $\boldsymbol{k}_b=k\hat{\boldsymbol{r}}_1$ and $\boldsymbol{k}_a=k\hat{\boldsymbol{r}}_0$,

$$\sum_s|F(\boldsymbol{k}_a,\boldsymbol{k}_b;\boldsymbol{k}_i)|^2\leqslant 2\sum_s[|f_s(\boldsymbol{k}_a,\boldsymbol{k}_b;\boldsymbol{k}_i)|^2+|f_s(\boldsymbol{k}_b,\boldsymbol{k}_a;\boldsymbol{k}_i)|^2]. \tag{41}$$

This follows from Eqs. (24) and (25) since we observe numerically that in sufficiently large calculations $F_s(k\hat{\boldsymbol{r}}_0,k\hat{\boldsymbol{r}}_1;\boldsymbol{k}_i)\approx 2f_s(k\hat{\boldsymbol{r}}_0,k\hat{\boldsymbol{r}}_1;\boldsymbol{k}_i)$. In such calculations, when plotted, the two sides of Eq. (41) are barely distinguishable. As for the hydrogen target, this is consistent with the interpretation that solving the close-coupling equations in the continuum is equivalent to taking a Fourier expansion of a step function [39]. Equation (41) also explains why the integral-preserving description for generating the cross sections given by [21] yielded a result too small by a factor of 2.

III. NUMERICAL METHOD

The details of the CCC method for electron-helium scattering utilizing an orthogonal Laguerre basis (CCC-L) have been given by [35]. Extension to using a box basis is relatively straightforward [43] as it is for the hydrogen target [4]. The two bases are fundamentally different. Upon diagonalization of the He^+ Hamiltonian, the first step of the He structure calculation utilizing the Laguerre basis leads to pseudostates that fall off exponentially governed by the parameter λ. The box basis, on the other hand, generates true He^+ eigenstates that fit within the box of size R_0, with the discretization of the continuum ensured by the boundary condition of the orbitals being zero at $r=R_0$. These orbitals are also set to zero for $r>R_0$. The primary differences in the orbitals occur at the larger values of r, as well as generating a different orbital energy distribution. Apart from the difference in the bases, for clarity of presentation, we shall keep other aspects of the CCC calculations the same, and independent of the incident energy. In particular, we set the maximum orbital angular momentum of the He^+ orbitals to $l_{\max}=5$. This results in 219 He states, leading to a maximum of 713 coupled channels.

The He states, used to define the multichannel expansion of the total e-He wave function, are defined in the following way. We restrict ourselves to the frozen-core model with the "inner" He electron described by the $1s$ He^+ orbital [35]. Hence, all states can be written as appropriately symmetrized $1snl$ configurations. These yield an excellent description of the He bound excited states as well as the one-electron ionization states leaving He^+ in the ground state. The biggest error occurs in the $1s1s'$ description of the ground state. The calculated ionization energy is 23.74 eV, which is 0.84 eV too low. We adjust for this by reducing the incident electron energy by 0.84 eV and therefore ensure the same excess energy used in the experiments. The lowest-energy orbitals are best obtained using large bases. This, however, generates too many states. We avoid this problem by diagonalizing the He Hamiltonian twice, the first time using a large set of He^+ orbitals and the second time using a smaller number of orbitals obtained from the first diagonalization. Specifically, having obtained around 100 He^+ orbitals, we diagonalize the He Hamiltonian for each ^1L symmetry and keep just the lowest-energy $20-l$ orbitals of the $1snl$ configurations. To ensure that the subsequent diagonalization will yield accurate ^3L states, we also keep the lowest two orbitals of the ^3S and ^3P diagonalization. This completes the first set of diagonalizations and leaves us with 23 s orbitals (including $1s$), 21 p orbitals, and $20-l$ orbitals for $2\leqslant l\leqslant l_{\max}$. Now the second set of He diagonalization is performed using all of these orbitals, resulting in 23, 21, 18, 17, 16, and 15 singlet states for $l=0$, 1, 2, 3, 4, and 5, respectively. The same number of triplet states are generated, except for one less in the ^3S symmetry, leading to a total of 219 states. The radial extent and target pseudostate energies in the CCC-L and CCC-B calculations are then controlled solely by λ and R_0, respectively.

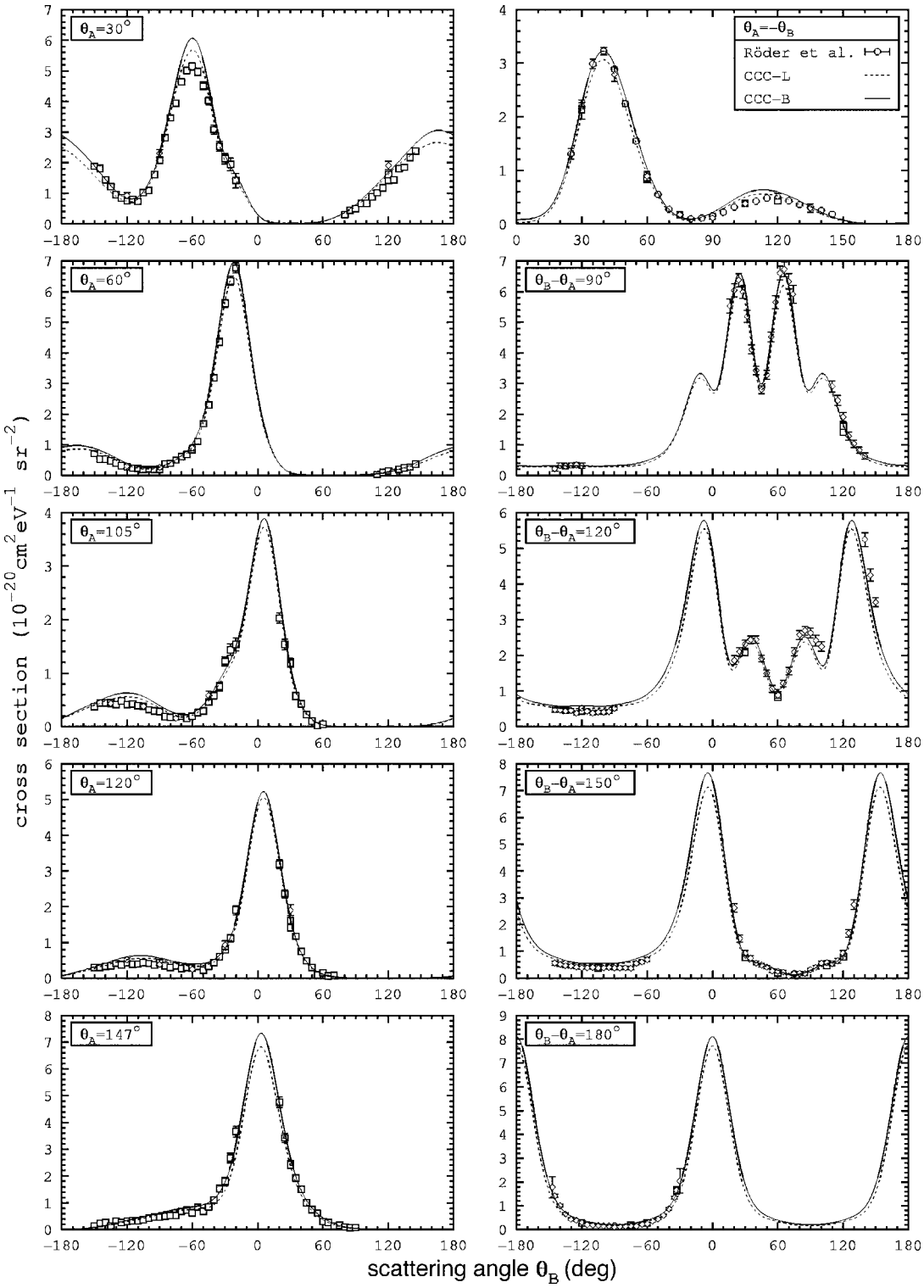

FIG. 1. Coplanar fully differential cross sections for 64.6 eV electron-impact single ionization of helium with 20 eV outgoing electrons. The published measurements of Röder *et al.*, which have an absolute uncertainty of around 25% [44], have been multiplied by 1.2 for a good visual fit to the CCC theory (see text).

IV. RESULTS

The application of the CCC theory to *e*-He doubly and singly differential, as well as total cross sections, has been recently discussed [45]. Here we focus on the special case of fully differential cross sections for equal-energy outgoing electrons. We begin at the highest energies for which experimental data are available and progress by moving towards the ionization threshold. For convenience, the convention

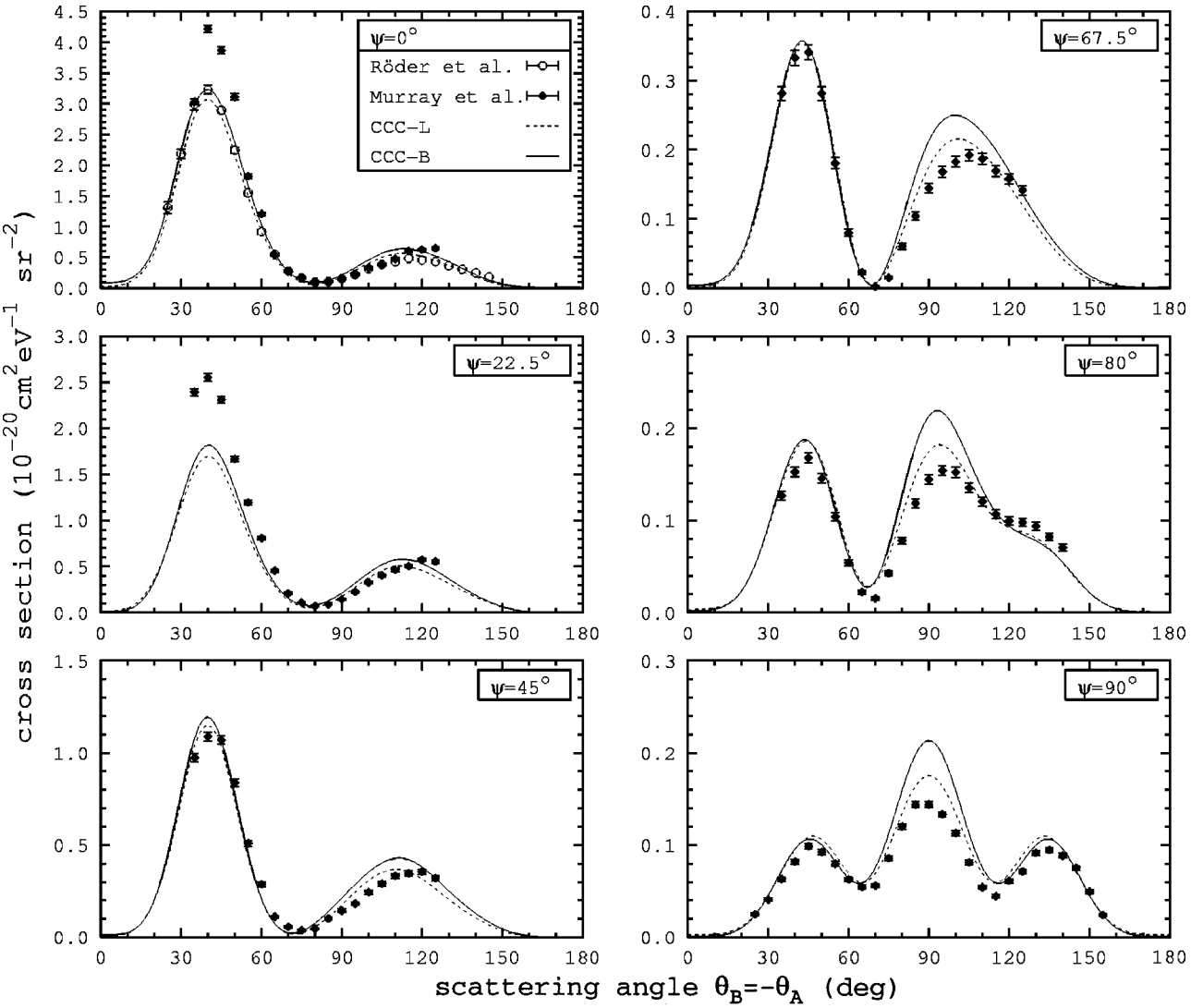

FIG. 2. Fully differential cross sections for out-of-plane, by angle ψ, 64.6 eV electron-impact single ionization of helium with 20 eV outgoing electrons. The measurements of Murray and Read [27] have been normalized to the corresponding Röder *et al.* data of Fig. 1 at $\theta_B=90°$, the common angle in the presented geometries. The CCC methods are described in the text.

that ejection angles on opposite sides of the incident beam have opposite signs is used throughout.

The in-plane and out-of-plane results for 64.6 eV incident energy with 20 eV outgoing electrons are given in Figs. 1 and 2, respectively. In Fig. 1, three geometries are considered: "fixed-θ_A" (squares), "symmetric" (circles), and "fixed-θ_{AB}" (diamonds). These are slices through the cross-section surface, which is a function of the positions of the two detectors at θ_A and θ_B. Different symbols are used to facilitate comparison between individual slices when they intersect. In the present case, we see excellent consistency in the measurements. There is also good agreement between the two theories and experiment. The latter has an uncertainty of 25% in the absolute values [44] and has been multiplied uniformly by 1.2 to obtain a good visual fit with experiment. The present CCC calculations are much larger than those given earlier [44], but yield substantially improved results only when the cross sections are small. [See, for example, Fig. (4) of Ref. [44].) Note also that the original CCC results presented were multiplied by 1.8. We now understand that they should have been multiplied by exactly 2, and hence the experimental data were multiplied by 1.2, as presently. The results obtained with the doubled incoherent combination of amplitudes and the coherent combination [see Eq. (41)] are barely distinguishable, and thus only the coherent result is plotted. The CCC-L and CCC-B calculations, see Sec. III, used $\lambda=6.2$ and $R_0=40.0$, respectively.

The geometry presented in Fig. 2 corresponds to the symmetric geometry of Fig. 1 when the angle of the electron gun relative to the plane is $\psi=0°$. As ψ is varied, the point at $\theta_B=-\theta_A=90°$ corresponds to the same geometrical arrangement and hence fixes the internormalization of the various geometries presented. This point is near the minimum of the cross section for $\psi=0°$, but it is the maximum for the case $\psi=90°$. This indicates the rapid fall of the cross sections as the incident beam approaches the so-called "perpendicular plane geometry," studied extensively by Murray *et al.* [26]. The measurements of Murray and Read [27] are relative and

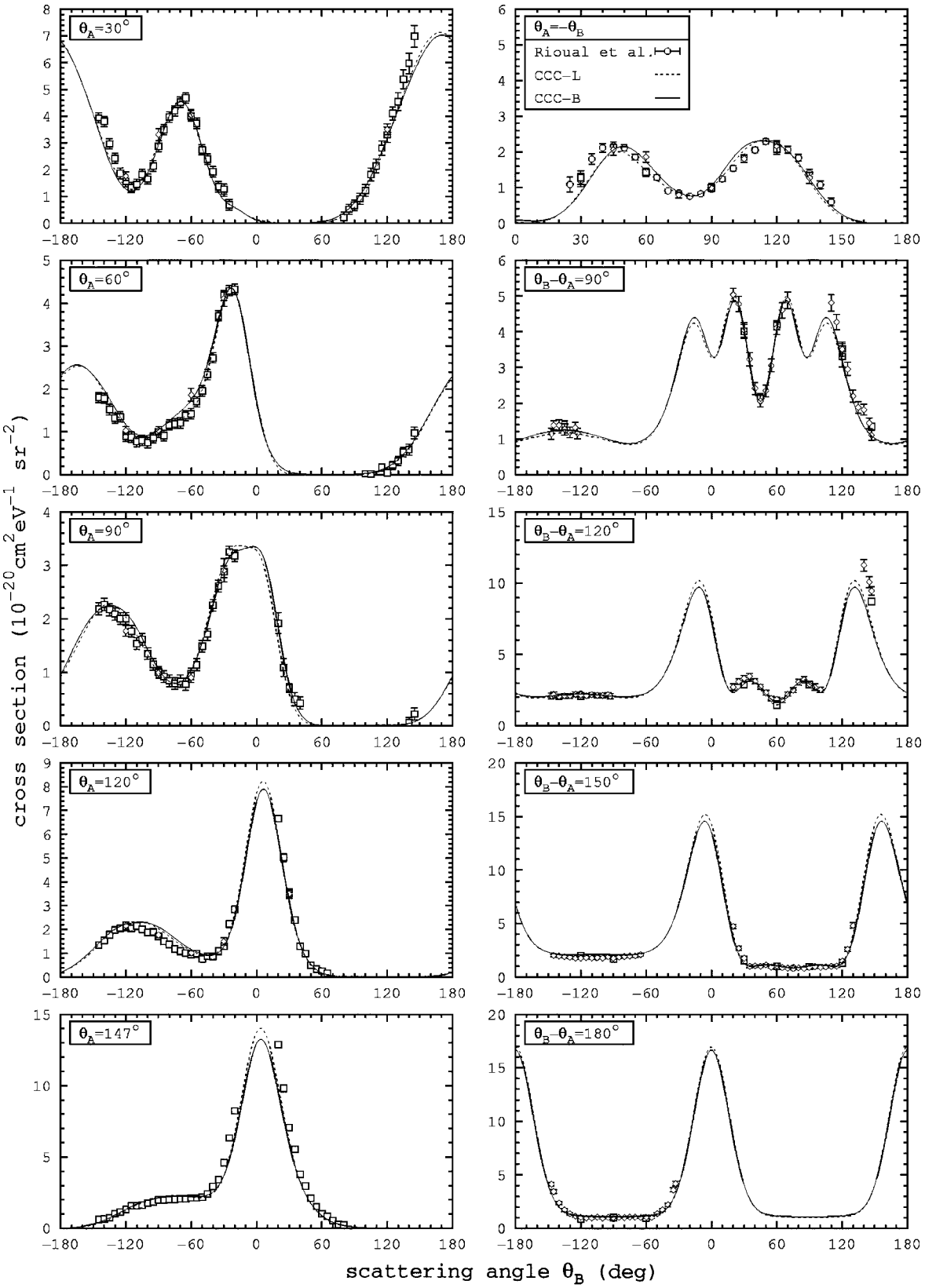

FIG. 3. Coplanar fully differential cross sections for 44.6 eV electron-impact single ionization of helium with 10 eV outgoing electrons. The measurements of Rioual *et al.* [28], which have an absolute uncertainty of approximately 25%, have been multiplied by 0.9 for a good visual fit to the CCC theory (see text).

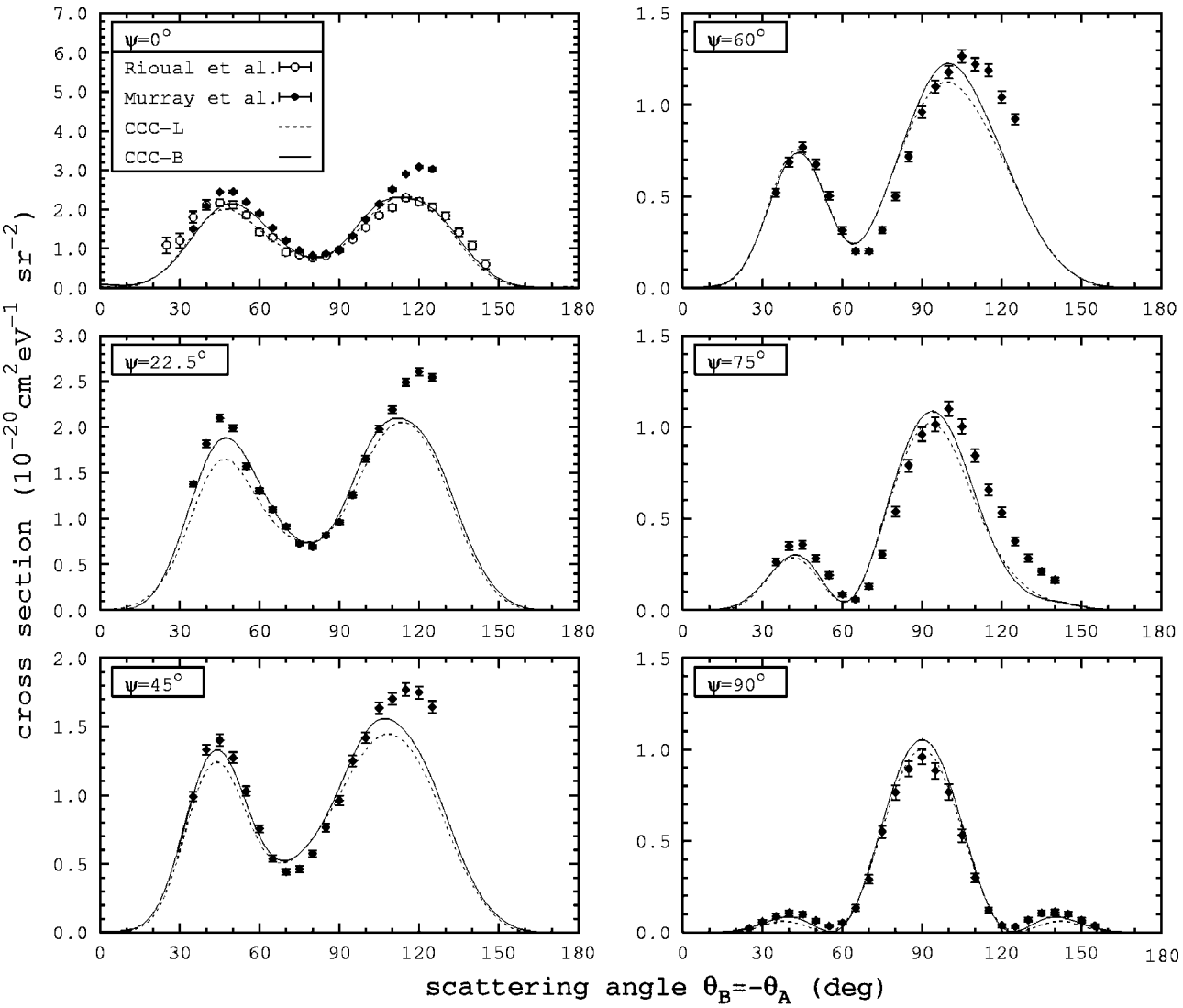

FIG. 4. Fully differential cross sections for out-of-plane, by angle ψ, 44.6 eV electron-impact single ionization of helium with 10 eV outgoing electrons. The measurements of Murray *et al.* [46] have been normalized to the corresponding Röder *et al.* data of Fig. 3 at $\theta_B = 90°$, the common angle in the presented geometries. The CCC models are described in the text.

we fix their absolute scale using the "symmetric" data of Fig. 1. In doing so, we see that, if we fix the two data sets at the $\theta_B = -\theta_A = 90°$ point, then there is some discrepancy near the maximum around $\theta_B = 40°$. Curiously, for $\psi \geqslant 45°$ this discrepancy between experiment and theory disappears. Given the smallness of the cross sections as ψ increases, the agreement between the two theories and experiment is very satisfactory.

Figures 3 and 4 are similar to those just discussed, except that the incident energy is 44.6 eV, with 10 eV outgoing electrons. The CCC-L and CCC-B calculations were run with $\lambda = 4.4$ and $R_0 = 41.0$, respectively. The coplanar data of Rioual *et al.* [28], with an absolute uncertainty of ±25%, show good internal consistency. After the published data were multiplied by 0.9, excellent agreement with the predictions from the two CCC theories is obtained. The same scaling factor was also used by Rioual *et al.* [28] when comparing with the earlier CCC calculations. The present results represent a small but still significant improvement over the previous predictions, particularly where the cross sections are small.

In Fig. 4, the corresponding out-of-plane data are presented, normalized at the $\theta_B = 90°$ point to the Rioual *et al.* [28] data. Once again we see a discrepancy between the two sets of measurements, with the theory being more supportive of the Rioual *et al.* [28] data. As ψ is increased, a small angular shift appears between theory and experiment. This shift disappears for the perpendicular plane geometry where the agreement between experiment and theory is excellent.

We next move considerably closer to the ionization threshold and consider 32.6 eV incident electrons with 4 eV outgoing electrons, presented in Fig. 5. As the threshold is approached, the required radial extent of the wave functions in the CCC calculations grows. Here the CCC-L and CCC-B calculations were performed with $\lambda = 2.9$ and $R_0 = 77.0$, respectively. Agreement between the two calculations and the experiment is once again excellent. The internal consistency of the experimental data is generally good, with some minor

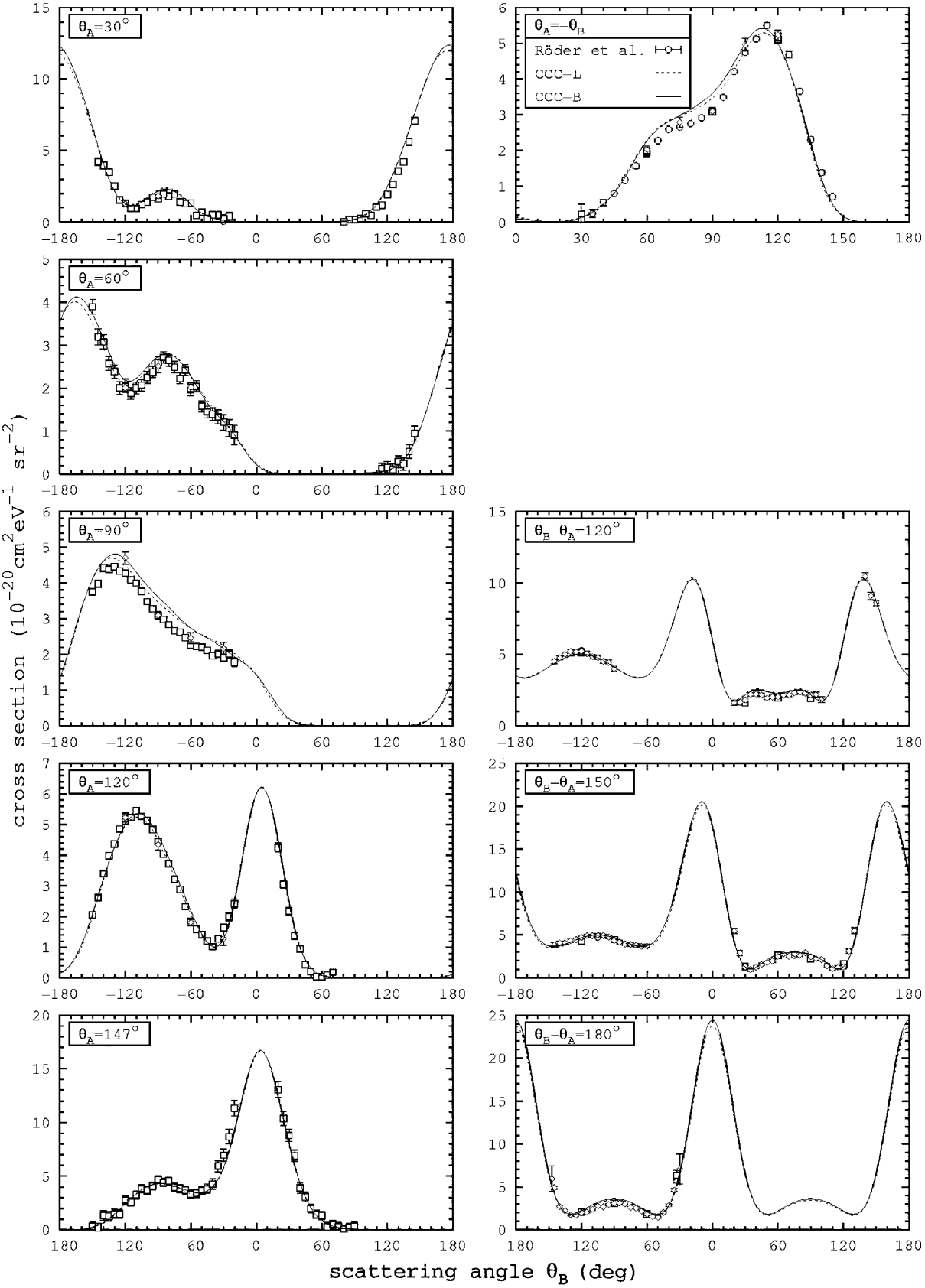

FIG. 5. Coplanar fully differential cross sections for 32.6 eV electron-impact single ionization of helium with 4 eV outgoing electrons. The measurements of Röder *et al.*, which have an absolute uncertainty of approximately 25% [47], have been multiplied by 0.9 for a good visual fit to the CCC theory (see text).

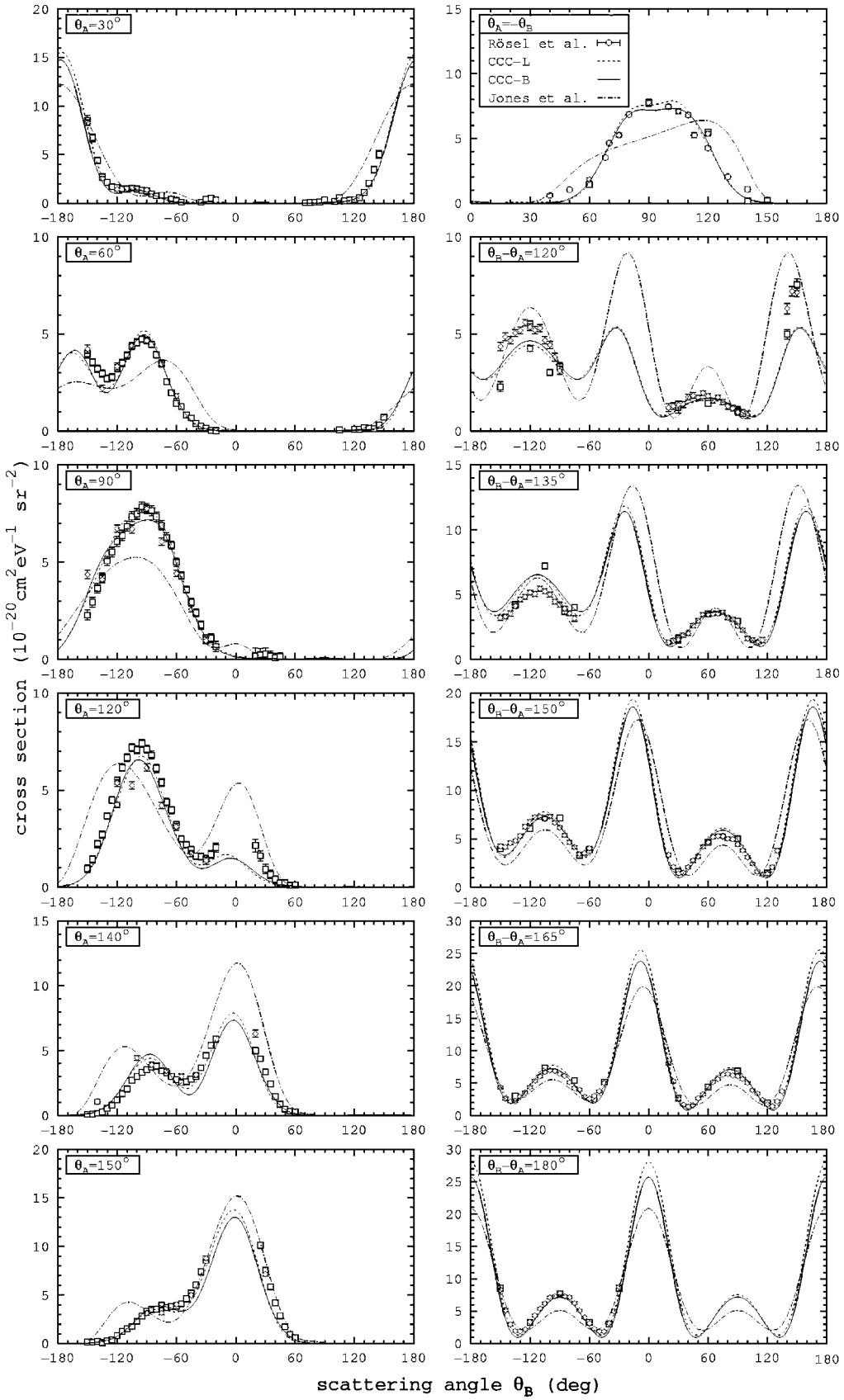

FIG. 6. Coplanar fully differential cross sections for 26.6 eV electron-impact single ionization of helium with 1 eV outgoing electrons. The absolute (±22%) measurements and the Jones *et al.* predictions are given by Rösel *et al.* [29]. The CCC models are described in the text.

exceptions, as seen, for example, in the $\theta_A=90°$ panel at $\theta_B=120°$. Particularly pleasing is the ability of theory to obtain negligible cross sections for the two electrons exiting in a similar direction (cf. Fig. 4 of Bray *et al.* [47]). The absolute values of the CCC theory are now clearly defined, unlike previously [47].

Finally, we consider the most difficult kinematic regime just above the ionization threshold. In Fig. 6, we present a comparison of the CCC predictions with the measurements of 26.6 eV incident electrons leading to 1 eV outgoing electrons. The CCC-L and CCC-B calculations were performed with $\lambda=2.06$ and $R_0=120.0$, respectively. The data of Rösel *et al.* [29], which we believe were taken with a different apparatus than that used for the corresponding higher-energy data, occasionally exhibit substantial internal inconsistency. One example, which shows a 50% discrepancy, is for $\theta_B=-150°$ on the $\theta_A=90°$ and $\theta_B-\theta_A=120°$ panels. Not all the points of inconsistency have been plotted. For example, the point at $\theta_A=30°$, $\theta_B=120°$ (top left panel), which agrees with the CCC theory, should be the same as the point at $\theta_B=30°$, $\theta_A=120°$, which is a factor of about 2 higher than the CCC result. Nevertheless, the overall agreement of the CCC calculations with experiment is good, both in shape and absolute value. We also compare with the DWBA results of Jones *et al.* [29]. Given that these calculations are based on the distorted-wave approach, they yield quite reasonable agreement with the experimental data and the CCC calculations at such a low energy.

V. SUMMARY AND CONCLUSIONS

In summary, we have presented the theory for extracting the ionization amplitudes from close-coupling-based *e*-He calculations, concentrating on the special kinematic case where the two outgoing electrons have equal energy. The innate symmetries of the underlying CCC amplitudes are the reason why the cross-section prescription given by Bray and Fursa [21] yielded such accurate angular distributions, but were a factor of 2 too low. Large-scale CCC calculations using both the Laguerre and box bases have been applied and shown to give excellent absolute agreement with experiment from near-threshold through to intermediate energies.

ACKNOWLEDGMENTS

This work was supported by the Australian Research Council (I.B., A.T.S., and D.V.F.) and by the U.S. National Science Foundation (K.B.). In particular, A.T.S. and K.B. would like to acknowledge an International Research Exchange (IREX) grant from the ARC.

APPENDIX

We now give some details of the stationary-phase results that are needed to discuss the ionization asymptotics. We make use of the integral identity

$$\int_0^K \phi(k)\mathrm{e}^{iRf(k)}dk \underset{R\to\infty}{\sim} \sqrt{\frac{2\pi}{Rf''(k_0)}}\phi(k_0)\mathrm{e}^{i[Rf(k_0)+\pi/4]} \quad \text{(A1)}$$

when $f'(k_0)=0$ is achieved for $k\in(0,K)$.

We consider integrals of the form

$$I=\int_0^K \phi(q)\mathrm{e}^{i(kr_1+qr_2)}dq \quad \text{(A2)}$$

and define $\tan\alpha\equiv r_2/r_1$, $R\equiv\sqrt{r_1^2+r_2^2}\to\infty$, $\tan\beta\equiv q/k$, and $K\equiv\sqrt{k^2+q^2}$. With these definitions,

$$I=\int_0^K \phi(q)\mathrm{e}^{iRK\cos[\alpha-\beta(q)]}dq. \quad \text{(A3)}$$

Hence,

$$f(k)=K\cos[\alpha-\beta(q)], \quad \text{(A4)}$$

$$f'(q)=0 \text{ if } q=k\tan\alpha, \quad \text{(A5)}$$

$$f''(q)=-\frac{K}{k^2}. \quad \text{(A6)}$$

Using Eq. (A1) in Eq. (A3) yields

$$I\underset{R\to\infty}{\sim}\phi(q)\left(\frac{2\pi}{KR}\right)^{1/2}k\mathrm{e}^{i(KR-\pi/4)} \quad \text{(A7)}$$

if $0<\alpha=\arctan(r_2/r_1)<\pi/2$ and $q=k\tan\alpha$.

Symbolically, we may write

$$\mathrm{e}^{i(kr_1+qr_2)}\underset{\substack{R\to\infty\\ \tan\alpha=r_2/r_1}}{\sim}\delta(\arctan(q/k)-\alpha)\left(\frac{2\pi}{KR}\right)^{1/2}k\mathrm{e}^{i(RK-\pi/4)}. \quad \text{(A8)}$$

To represent the ejected electrons, we use continuum waves $\phi_{\boldsymbol{k}}^{(-)}$ [normalized to $\delta(\boldsymbol{k}-\boldsymbol{k}')$] with incoming scattered waves,

$$\phi_{\boldsymbol{k}}^{(-)}\underset{r\to\infty}{\sim}(2\pi)^{-3/2}\left[\mathrm{e}^{i[\boldsymbol{k}\cdot\boldsymbol{r}+(1/k)\ln(kr+\boldsymbol{k}\cdot\boldsymbol{r})]}+\frac{\mathrm{e}^{-i[kr+(1/k)\ln(kr)]}}{r}f(-k\hat{\boldsymbol{r}})\right]. \quad \text{(A9)}$$

Furthermore, in this limit we may use

$$\mathrm{e}^{i\boldsymbol{k}\cdot\boldsymbol{r}}\underset{r\to\infty}{\sim}=\frac{2\pi}{ik}\left[\frac{\mathrm{e}^{ikr}}{r}\delta(\hat{\boldsymbol{k}}-\hat{\boldsymbol{r}})-\frac{\mathrm{e}^{-ikr}}{r}\delta(\hat{\boldsymbol{k}}+\hat{\boldsymbol{r}})\right]. \quad \text{(A10)}$$

Thus the component of $\phi_{\boldsymbol{k}}^{(-)}(\boldsymbol{r})$ with an outgoing spherical wave is

$$\phi_{\boldsymbol{k}}^{(-)\mathrm{out}}(\boldsymbol{r})\underset{r\to\infty}{\sim}=\frac{(2\pi)^{-1/2}}{ikr}\mathrm{e}^{i[kr+(1/k)\ln(2kr)]}\delta(\hat{\boldsymbol{k}}-\hat{\boldsymbol{r}}). \quad \text{(A11)}$$

For ionization processes in the coupled channels formalism, we need to consider integrals of the form

$$\Psi(\boldsymbol{r}_1,\boldsymbol{r}_2) \underset{r_1,r_2\to\infty}{\sim} \int_0^{\sqrt{2E}} d^3q\,\phi_{\boldsymbol{q}}^{(-)}(\boldsymbol{r}_2)\frac{e^{ikr_1}}{r_1} f(k\hat{\boldsymbol{r}}_1, q\hat{\boldsymbol{r}}_2;\boldsymbol{k}_0)$$

$$\underset{r_1,r_2\to\infty}{\sim} \int_0^{\sqrt{2E}} d^3q \frac{(2\pi)^{-1/2}}{iq}\delta(\hat{\boldsymbol{q}}-\hat{\boldsymbol{r}}_2)\frac{e^{i(kr_1+qr_2)}}{r_1r_2} \times e^{i(1/k)\ln(2kr_2)} f(k\hat{\boldsymbol{r}}_1, q\hat{\boldsymbol{r}}_2;\boldsymbol{k}_0)$$

$$\underset{r_1,r_2\to\infty}{\sim} -i\int_0^{\sqrt{2E}} dqq\,\delta(q-k\tan\alpha) \times \left(\frac{1}{KR}\right)^{1/2} \frac{ke^{i(KR-\pi/4)}}{r_1r_2} e^{i(1/k)\ln(2kr_2)} f(k\hat{\boldsymbol{r}}_1, q\hat{\boldsymbol{r}}_2;\boldsymbol{k}_0) \quad \text{(A12)}$$

and therefore

$$\Psi(\boldsymbol{r}_1,\boldsymbol{r}_2) \underset{r_1,r_2\to\infty}{\sim} e^{-i3\pi/4}\frac{K^{3/2}}{R^{5/2}} e^{iKR} f(k\hat{\boldsymbol{r}}_1, q\hat{\boldsymbol{r}}_2;\boldsymbol{k}_0). \quad \text{(A13)}$$

In the last equation, we made use of the relation $q/r_2 = k/r_1 = K/R$, which follows from the stationary point condition $q/k = r_2/r_1$ and the definitions of K and R.

[1] J. Röder, H. Ehrhardt, C. Pan, A. F. Starace, I. Bray, and D. V. Fursa, Phys. Rev. Lett. **79**, 1666 (1997).
[2] J. Röder, J. Rasch, K. Jung, C. T. Whelan, H. Ehrhardt, R. J. Allan, and H. R. J. Walters, Phys. Rev. A **53**, 225 (1996).
[3] J. Röder, M. Baertschy, and I. Bray, Phys. Rev. A **67**, 010702(R) (2003).
[4] I. Bray, K. Bartschat, and A. T. Stelbovics, Phys. Rev. A **67**, 060704(R) (2003).
[5] I. Bray, J. Phys. B **32**, L119 (1999).
[6] M. Baertschy, T. N. Rescigno, and C. W. McCurdy, Phys. Rev. A **64**, 022709 (2001).
[7] M. Brauner, J. S. Briggs, and H. Klar, J. Phys. B **22**, 2265 (1989).
[8] J. Berakdar and H. Klar, J. Phys. B **26**, 3891 (1993).
[9] J. Berakdar and J. S. Briggs, Phys. Rev. Lett. **72**, 3799 (1994).
[10] S. Jones, D. H. Madison, and D. A. Konovalov, Phys. Rev. A **55**, 444 (1997).
[11] J. Berakdar, J. S. Briggs, I. Bray, and D. V. Fursa, J. Phys. B **32**, 895 (1999).
[12] C. T. Whelan, R. J. Allan, J. Rasch, H. R. J. Walters, X. Zhang, J. Röder, K. Jung, and H. Ehrhardt, Phys. Rev. A **50**, 4394 (1994).
[13] S. Jones, D. H. Madison, A. Franz, and P. L. Altick, Phys. Rev. A **48**, R22 (1993).
[14] A. Prideaux and D. H. Madison, Phys. Rev. A **67**, 052710 (2003).
[15] M. A. Haynes, B. Lohmann, A. Prideaux, and D. H. Madison, J. Phys. B **36**, 811 (2003).
[16] A. Prideaux and D. H. Madison, J. Phys. B **37**, 4423 (2004).
[17] T. N. Rescigno, M. Baertschy, W. A. Isaacs, and C. W. McCurdy, Science **286**, 2474 (1999).
[18] P. L. Bartlett, A. T. Stelbovics, and I. Bray, J. Phys. B **37**, L69 (2004).
[19] M. S. Pindzola and D. R. Schultz, Phys. Rev. A **53**, 1525 (1996).
[20] M. S. Pindzola and F. J. Robicheaux, Phys. Rev. A **61**, 052707 (2000).
[21] I. Bray and D. V. Fursa, Phys. Rev. A **54**, 2991 (1996).
[22] I. Bray, Phys. Rev. Lett. **89**, 273201 (2002).
[23] I. Bray, J. Phys. B **36**, 2203 (2002).
[24] A. S. Kadyrov, A. M. Mukhamedzhanov, A. T. Stelbovics, and I. Bray, Phys. Rev. Lett. **91**, 253202 (2003).
[25] A. S. Kadyrov, A. M. Mukhamedzhanov, A. T. Stelbovics, and I. Bray, Phys. Rev. A **70**, 062703 (2004).
[26] A. J. Murray, M. B. J. Woolf, and F. H. Read, J. Phys. B **25**, 3021 (1992).
[27] A. J. Murray and F. H. Read, J. Phys. B **26**, L359 (1993).
[28] S. Rioual, J. Röder, B. Rouvellou, H. Ehrhardt, A. Pochat, I. Bray, and D. V. Fursa, J. Phys. B **31**, 3117 (1998).
[29] T. Rösel, J. Röder, L. Frost, K. Jung, H. Ehrhardt, S. Jones, and D. H. Madison, Phys. Rev. A **46**, 2539 (1992).
[30] T. Rösel, C. Dupre, J. Röder, A. Duguet, K. Jung, A. Lahmam-Bennani, and H. Ehrhardt, J. Phys. B **24**, 3059 (1991).
[31] J. Röder, H. Ehrhardt, I. Bray, D. V. Fursa and I. E. McCarthy, J. Phys. B **29**, L67 (1996).
[32] J. Röder, H. Ehrhardt, I. Bray, D. V. Fursa and I. E. McCarthy, J. Phys. B **29**, 2103 (1996).
[33] J. Röder, H. Ehrhardt, C. Pan, A. F. Starace, I. Bray, and D. V. Fursa, J. Phys. B **31**, L525 (1998).
[34] I. Bray and A. T. Stelbovics, Phys. Rev. A **46**, 6995 (1992).
[35] D. V. Fursa and I. Bray, Phys. Rev. A **52**, 1279 (1995).
[36] I. Bray and D. V. Fursa, Phys. Rev. Lett. **76**, 2674 (1996).
[37] I. Bray, Phys. Rev. Lett. **78**, 4721 (1997).
[38] I. Bray and A. T. Stelbovics, Phys. Rev. Lett. **70**, 746 (1993).
[39] A. T. Stelbovics, Phys. Rev. Lett. **83**, 1570 (1999).
[40] I. Bray, J. Phys. B **33**, 581 (2000).
[41] I. Bray, D. V. Fursa, and A. T. Stelbovics, Phys. Rev. A **63**, 040702(R) (2001).
[42] R. K. Peterkop, *Theory of Ionization of Atoms by Electron Impact* (Colorado Associated University Press, Boulder, 1977).
[43] I. Bray, K. Bartschat, D. V. Fursa, and A. T. Stelbovics, J. Phys. B **36**, 3425 (2003).
[44] I. Bray, D. V. Fursa, J. Röder, and H. Ehrhardt, J. Phys. B **30**, L101 (1997).
[45] I. Bray, D. V. Fursa, and A. T. Stelbovics, J. Phys. B **36**, 2211 (2003).
[46] A. J. Murray, F. H. Read, and N. J. Bowring, Journal de Physique IV **3**, 51 (1993).
[47] I. Bray, D. V. Fursa, J. Röder, and H. Ehrhardt, Phys. Rev. A **57**, R3161 (1998).